Direct proton decay from the Gamow-Teller resonance in ^{208}Bi

H. Akimune,[1] I. Daito,[1] Y. Fujita,[2] M. Fujiwara,[1] M.B. Greenfield,[3] M.N. Harakeh,[4] T. Inomata,[2] J. Jänecke,[5] K. Katori,[2] S. Nakayama,[6] H. Sakai,[7] Y. Sakemi,[1,*] M. Tanaka,[8] and M. Yosoi[9]

[1]*Research Center for Nuclear Physics, Osaka University, Suita, Osaka 567, Japan*

[2]*Department of Physics, Osaka University, Toyonaka, Osaka 560, Japan*

[3]*Natural Science Division, International Christian University, Mitaka, Tokyo 181, Japan*

[4]*Kernfysisch Versneller Instituut, Zernikelaan 25, 9747 AA Groningen, The Netherlands*

[5]*Department of Physics, University of Michigan, Ann Arbor, Michigan 48109*

[6]*Department of Physics, Tokushima University, Tokushima, Japan*

[7]*Department of Physics, University of Tokyo, Bunkyoku, Tokyo 113, Japan*

[8]*Kobe Tokiwa Jr. College, Nagataku, Kobe 653, Japan*

[9]*Department of Physics, Kyoto University, Kyoto 606-01, Japan*

(Received 24 April 1995)

Spin-isospin excitations in ^{208}Bi have been investigated using the ^{208}Pb(^{3}He,t)^{208}Bi reaction at and near $\theta \approx 0°$ at $E(^3\text{He})$=450 MeV. The microscopic structure of the Gamow-Teller resonance (GTR), the isobaric analog state (IAS), and the spin-flip dipole ($\Delta L = 1$) resonance (SDR) in ^{208}Bi has been studied by observing their direct proton decays to the low-lying neutron-hole states in ^{207}Pb. Decay protons were measured at backward angles in coincidence with tritons detected at and near 0°. The total branching ratio for proton decay from the GTR is determined to be only 4.9±1.3%. The total branching ratio for proton decay from the SDR amounts to 14.1±4.2%. The deduced total widths as well as the total and partial proton escape widths of the GTR and IAS are found to be in reasonable agreement with recent theoretical estimates obtained in the framework of the continuum Tamm-Dancoff approximation.

PACS number(s): 24.30.Cz, 25.55.Kr, 27.80.+w, 29.30.Aj

I. INTRODUCTION

The Gamow-Teller resonance (GTR) was predicted in 1963 and was invoked to explain the retardation of Gamow-Teller transitions in β decay compared with single-particle estimates [1,2]. The existence of the GTR was first reported experimentally [3] in 1975 in the ^{90}Zr(p,n) reaction at the incident proton energy of 35 MeV. Historically, the presence of broad resonances corresponding to the GTR had already been seen by Bowen *et al.* [4] in 1962 in 0° (p,n) spectra measured for natural copper, lead, and uranium targets at E_p=143 MeV. However, the authors did not recognize the significance of the broad resonances observed in their (p,n) measurements, since the GTR was not theoretically predicted until a year later. In addition, this resonance was incorrectly interpreted as an isobaric analog state (IAS) [5].

In 1980, it was found that the GTR is preferentially excited at 0° in the ^{90}Zr$(p,n)^{90}$Nb reaction at the bombarding energy of 120 MeV [6]. Systematic studies of GTR's excited via (p,n) reactions were performed in the following years on numerous target nuclei across the Periodic Table at the Indiana University Cyclotron Facility [6–11]. Subsequently, it was suggested [10] that the Gamow-Teller strengths, empirically observed in heavy nuclei, exhausted only about 60–70 % of the model-independent sum rule of $3(N-Z)$ [1,12].

The GTR, characterized by a transferred isospin, spin, and angular momentum of $\Delta T = 1$, $\Delta S = 1$, and $\Delta L = 0$, respectively, is excited primarily via the central spin-isospin term in the effective nucleon-nucleon interaction, $V_{\sigma\tau}$. The isovector spin-flip dipole resonance (SDR), which is characterized by $\Delta T = 1$, $\Delta S = 1$, and $\Delta L = 1$ transfer, is also excited via the $V_{\sigma\tau}$ interaction. These spin-flip dipole resonances were predicted to explain the reduced strengths of first-forbidden β decay [13], and they were observed [10] via the (p,n) reaction at finite scattering angles. The IAS, characterized by $\Delta T = 1$, $\Delta S = 0$, and $\Delta L = 0$ transfer, is excited primarily via the central isospin term, V_τ. According to the effective nucleon-nucleus interaction theory [14,15], the ratio of the volume integrals of the spin-isospin and isospin terms, $|J_{\sigma\tau}/J_\tau|$, depends strongly on the bombarding energy. The ratio increases with increasing energy, reaches a maximum at ~300 MeV/u, and decreases gradually in the energy region from ~500 MeV to ~800 MeV. Thus, Gamow-Teller transitions are preferentially excited as compared to Fermi transitions [16–18] in the bombarding energy interval of 150–500 MeV. In addition, in this interval the isoscalar interaction, V_0, is relatively weak [14,15].

The wave functions of giant resonances excited via (p,n)-type charge-exchange reactions may largely be described as a coherent sum of the dominant one-neutron-hole–one-proton-particle ($1p$-$1h$) configurations. The decay of these resonances usually proceeds via particle de-

*Present address: Department of Physics, Tokyo Institute of Technology, Meguro-ku, Tokyo 152, Japan.

cay, since these resonances are above the particle decay threshold. Two mechanisms contribute to these particle decay processes: direct decay and statistical decay [19]. The direct decay occurs via emission of a proton particle leaving the daughter nucleus in a neutron-hole state. In this case the emitted proton carries valuable information about the $1p$-$1h$ wave function of the giant resonance. Statistical decay occurs through the coupling of the $1p$–$1h$ configurations to the $2p$-$2h$ and more complicated configurations. In heavy nuclei, this mainly leads to the emission of neutrons, because emission of protons is strongly suppressed by the Coulomb barrier. For example, statistical neutron decay is favored by about three orders of magnitude over statistical proton decay for particle emission from the GTR in ^{208}Bi .

The situation sketched above suggests that proton decay from a GTR carries information about the damping mechanism of this GTR. Furthermore the theoretical evaluation of the branching ratios for the direct proton decays to residual neutron-hole states should elucidate detailed aspects of the $1p$-$1h$ microscopic structure of the GTR. However, experimental limitations presented an obstacle for such investigations for a long time. A coincidence measurement of proton decay from the GTR excited via the (p,n) reaction at intermediate energies suffers from two experimental difficulties: low efficiency and low-energy resolution inherent to neutron detection at intermediate energies. These difficulties are compounded since the low neutron detection efficiency necessitates the use of thick targets, causing further difficulties in detecting the low-energy decay protons because of energy loss and straggling in the thick target.

The (^{3}He,t) reaction is more favorable to investigate the microscopic structure of the GTR, because of the high detection efficiency for the emitted tritons and of the energy resolution attainable by using a magnetic spectrometer. At intermediate bombarding energies ($\geq$ 100 MeV/u), the (^{3}He,t) reaction preferentially excites spin-flip levels via $V_{\sigma\tau}$ at 0° [20,21], and the reaction mechanism is relatively simple compared to that at lower bombarding energies ($\leq$ 100 MeV/u).

The first attempt to study the proton decay from states in ^{208}Bi was undertaken by Gaarde *et al.* [22] making use of the (^{3}He,t) reaction, whereby the tritons were detected at 0° with a magnetic spectrometer. However, the ^{3}He-bombarding energy of 27 MeV/u was too low to appreciably excite spin-flip states [23,24]. The observed proton decay from the region of the GTR to the neutron-hole states in ^{207}Pb accounted for essentially the total decay of the GTR, which was quite surprising, since the total observed width of the GTR of $\sim$4 MeV in ^{208}Bi would thus be entirely due to the escape width $\Gamma^{\uparrow}$. The data were in strong disagreement with the theoretical calculation by Van Giai *et al.* [25] by more than an order of magnitude.

In addition to proton decay of the GTR, two mechanisms are believed to contribute to this strong population of the neutron-hole states in the experiment by Gaarde *et al.* at 27 MeV/u [22]. They arise from the low bombarding energy employed in the experiment. The kinematics of the breakup-pickup process, (^{3}He,dp)(d,t), provides a high energy tail of tritons at this bombarding energy, which interferes with tritons from the excitation of the GTR. Since this two-step reaction is mediated by neutron pickup to the neutron-hole states in ^{207}Pb, its contribution may mask the GTR proton decay into these states. Furthermore, the complex reaction mechanism may play a role at the low bombarding energies and can lead to the excitation of non-spin-flip states which have a very high level density at the high excitation energies of interest. Both mechanisms are much less probable for the (^{3}He,t) charge-exchange reaction at the higher bombarding energy of 450 MeV.

There is, at present, considerable theoretical interest in the damping mechanism of the GTR and in particular in its escape width resulting from its microscopic structure. Theoretical predictions for the escape width associated with proton decay depend on the microscopic model and the residual nucleon-nucleon interaction used in the nuclear structure calculations. Thus, the precise determination of partial proton decay widths will provide a measure to differentiate between various theoretical models and/or the employed residual interactions. This may help to solve the longstanding problem of the quenching of the GTR strength.

In the present work, we present a detailed description of the proton-decay measurements from the spin-isospin resonances in ^{208}Bi. Preliminary results from these measurements have been reported elsewhere [26].

II. EXPERIMENT

The experiment was carried out at the Research Center for Nuclear Physics (RCNP) Osaka University. A ^{3}He^{++} beam accelerated to 90.1 MeV with the AVF cyclotron was injected into the K = 400 MeV ring cyclotron [27], and further accelerated to 450 MeV. The beam extracted from the ring cyclotron was achromatically transported to the ^{208}Pb target with a thickness of 5.2 mg/cm^2 (99.86% isotopic enrichment). The typical beam intensity was 2 nA (electrical), and the energy resolution of the beam was about 300 keV. The beam spot size on the target was about 1 mm × 1 mm. The emittance of the beam was $\sim$2 mrad (FWHM). The halo of the beam was monitored by measuring the counting rates in plastic scintillators arranged at several points along the beam transport line from the ring cyclotron to the target.

A. Singles measurement

Measurements of the ^{208}Pb(^{3}He,t)^{208}Bi reaction were made using the magnetic spectrometer "Grand Raiden" [28]. Due to the high magnetic rigidity (K = 1.42 GeV), tritons with a maximum energy of 470 MeV can be measured. The spectrometer covers a momentum range of $\Delta p/p$ = 5% over the focal-plane length of 1.2 m. The horizontal and vertical magnifications are $M_x = -0.417$ and $M_y = 5.98$, respectively. A schematic

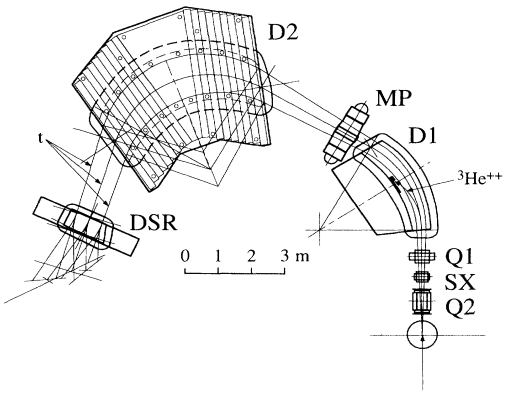

FIG. 1. Top schematic view of the spectrometer Grand Raiden. The ^{3}He^{++} beam was stopped at the Faraday cup placed at the inside wall of the D1 magnet.

picture of the Grand-Raiden spectrometer is shown in Fig. 1. This spectrometer consists of two dipole magnets (D1, D2), two quadrupole magnets (Q1, Q2), and one sextupole (SX) magnet. In addition to these magnets, one multipole magnet (MP) is located between the D1 and D2 magnets for correction of the kinematic energy-broadening effects.

The spectrometer was set at $-0.3°$ to measure tritons emitted at angles of 0° and 1° simultaneously. The opening angles, which were defined by a slit at the entrance of the spectrometer, were ±20 mrad horizontally, and ±20 mrad vertically. The spectrometer covered an angular range from $-1.45°$ to 0.85°. In addition, the spectrometer was rotated towards larger angles, and singles ^{208}Pb(^{3}He,t) measurements were performed at θ=3° and 5°. The transmission of scattered particles passing through the spectrometer with this solid angle was confirmed to be 100% in other (p,p') and (^{3}He,^{3}He′) measurements performed independently.

The incident ^{3}He^{++} beam was stopped by a Faraday cup positioned at the inside of the D1 magnet. Tritons from the (^{3}He,t) charge-exchange reaction having a higher magnetic rigidity were separated by the spectrometer from the incident ^{3}He^{++} beam and other reaction products such as breakup protons and deuterons. The magnetic fields of D1 and D2 were fixed at about 1.8 T. The stability of the magnetic field was kept within 3×10^{-5} T during the entire period of the experiment.

The ejectile tritons were detected with two multiwire drift chambers (MWDC's) [29] placed along the focal plane with a tilting angle of 45° with respect to the central orbit of the spectrometer. The MWDC's were 1150 mm long and 45 mm high. One MWDC was placed at the focal plane of the spectrograph, and the other MWDC was placed at a distance of 250 mm downstream from the first one. Each MWDC consisted of two planes: one was sensitive to measure horizontal positions of the incident charged particles, and the other was sensitive to the vertical positions. The spacing of the sense wires was 4 mm. The maximum drift length of electrons was 10 mm. Incident charged particles passing through four or five drift cells generated in a scintillator the start timing signals to measure the drift times of electrons moving from the ionization track towards the sense wires. The position and angular resolutions of the MWDC's were 0.3 mm and 1.2 mrad, respectively.

The MWDC's were backed by two ΔE plastic scintillators with a thickness of 5 mm each. These scintillators were used for particle identification, as well as for generating trigger signals for coincidence events and stop-timing signals for the MWDC's.

B. Coincidence measurement

Decay protons following the (^{3}He,t) reactions were detected by a set of eight lithium-drifted silicon detectors (SSD) with a thickness of 5 mm and an effective area of 400 mm^2 each. The 5 mm thick SSD allows the detection of protons with energies up to 30 MeV. Four SSD's were located at the scattering angle of 132° in the laboratory system, and the other four at 157°, with azimuthal angles of 45°, 135°, 225°, and 315° with respect to the beam direction, respectively. The total solid angle for proton detection covered by the SSD array was 3.3%. A schematic picture of the layout of the SSD's is shown in Fig. 2.

The energy threshold for each SSD was set at 500 keV, well above noise-level signals. No particle identification was needed because energetic particles, such as ^{3}He particles from elastic scattering, deuterons from breakup processes, or protons from quasifree processes, were strongly forward peaked. These energetic particles do not give true coincidence signals for the excitation-energy region of interest. Furthermore, since charged-particle decay from the excited states in ^{208}Bi is suppressed by the Coulomb barrier, contributions from α decay were negligible. Therefore, a ΔE counter for particle identification was not needed.

A gate with a timing width for the coincidence measurements of tritons and protons was set at 500 ns to allow the measurement of prompt and random events. The count rates for signals from the focal-plane detector, and from each SSD were about 600 cps and 5 kcps, respectively. Coincidence signals between the focal-plane

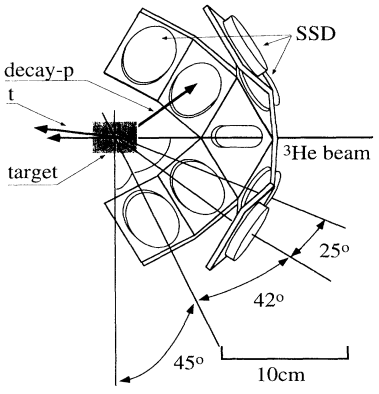

FIG. 2. Schematic picture of the layout of the SSD's.

detector and SSD's, and prescaled (factors 1/2 or 1/3) signals from the focal-plane detector alone triggered the data-acquisition system.

III. DATA REDUCTION

A position spectrum of tritons obtained with the focal-plane detector system was converted to an energy spectrum. The conversion coefficients were determined using the peak positions for known excited states in ^{12}N and ^{13}N from the ^{nat}C(^{3}He,t)N reaction. The reaction with the natural carbon target was measured to calibrate the focal-plane position and to test the coincidence electronics. The Q values for all observed excited states in ^{12}N and ^{13}N were well reproduced by using a linear function of the measured focal-plane positions.

The particle identification spectrum was obtained from the plastic scintillators. It showed no obvious experimental background except for singly ionized ^{3}He$^+$ particles. These ^{3}He$^+$ particles were due to the atomic-charge exchange reaction in the ^{208}Pb target [30]. The ratio of the fraction of ions Y(^{3}He$^+$)/Y(^{3}He^{++}) was $\sim 9\times10^{-9}$. The energy distribution and the angular distribution of these ^{3}He$^+$ particles are identical to those of the incident ^{3}He^{++} beam. Thus, the ^{3}He$^+$ particles provide a calibration for both the energy and the 0° angle of the incident ^{3}He beam at 450 MeV. This capability to monitor the energy of the incident ^{3}He^{++} beam was particularly important because of energy drifts over extended periods of time. The energy of the incident ^{3}He^{++} beam (relative values) was determined by averaging the observed energies of the ^{3}He$^+$ particles every five seconds during the experiment (~500 events each). Energy drifts of the incident beam over a period of 14 d were observed to be in the range of about 2 MeV. The triton energies were corrected by taking into account the energy drift of the incident beam monitored by the peak for the ^{3}He$^+$ particles. By employing the above energy correction procedure, the energy resolution of the singles triton spectra from the ^{208}Pb(^{3}He,t) reaction could be improved to ~300 keV.

The scattering angles for the tritons were determined by tracing back their positions and angles of incidence at the focal plane. The uncertainties in determining the incident triton angles were 3 mrad and 10 mrad for the horizontal and vertical directions, respectively. Both angular uncertainties are partly due to the emittance of the incident ^{3}He beam. The vertical angular uncertainty was worse than the horizontal one, because the vertical magnification of the spectrometer is much larger than the horizontal magnification.

Figure 3 shows a three-dimensional plot wherein the number of counts is shown for the triton energy versus scattering angle. The prominent peak at 450 MeV corresponds to the singly ionized ^{3}He$^+$ particles. It is evident that the cross sections for the Gamow-Teller resonance and the isobaric analog state increase sharply towards 0°, whereas the spin-flip dipole resonance (SDR), excited with a transferred angular momentum of $\Delta L = 1$, is peaked at ~1°. Figure 4 shows triton energy spectra for angles of ~0° and ~1°. The two spectra were obtained

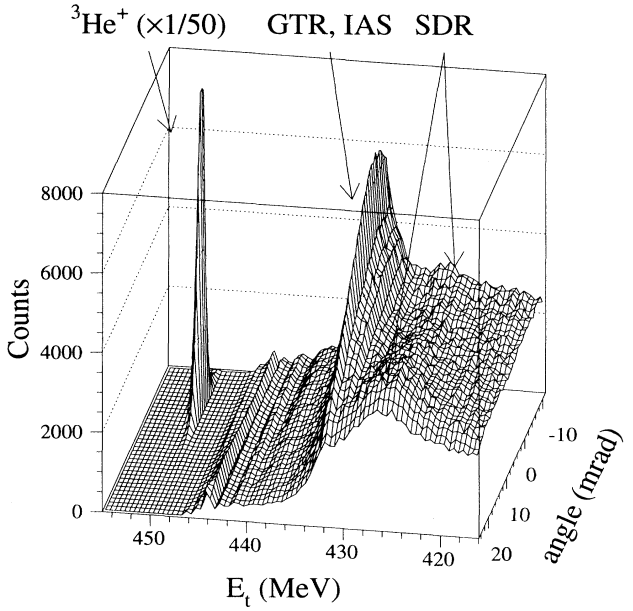

FIG. 3. Three-dimensional plot for the number of counts as a function of the triton energy versus scattering angle from the ^{208}Pb(^{3}He,t) reaction at E(^{3}He)=450 MeV. The prominent peak at 450 MeV corresponds to events due to ^{3}He$^+$ particles resulting from the atomic charge-exchange reaction on the ^{208}Pb target. The broad bump at $E_t \approx 433$ MeV corresponds to the Gamow-Teller resonance (GTR) and the isobaric analog state (IAS) in ^{208}Bi. The two bumps at around $E_t \approx 428$ MeV which are seen at $\theta \simeq 1°$ correspond to the spin-flip dipole resonance (SDR) excited with a transferred angular momentum of $\Delta L = 1$.

by applying software gates with solid angles of 0.28 msr centered at 0° and 1°. The results of the decomposition into various resonances and continuum background are also plotted.

The time interval between two beam bursts from the ring cyclotron was 84 ns. The gate width of the coincidence circuit for coincidences between triton and proton events was set at 500 ns. Figure 5 shows a timing spectrum for the proton-triton coincidence events. The prominent peak at the center of the histogram in Fig. 5 corresponds to prompt coincidence events. The small peaks correspond to events due to random coincidences. The ratio of prompt to random coincidences was about 4. After applying a software gate to obtain coincidence events for the final excited states in ^{207}Pb (E_x = 0-4 MeV), the ratio increased to more than 10 (see Fig. 5). True coincidence spectra were obtained by subtracting the random coincidence spectra from the prompt ones. The statistical error caused by this subtraction was less than 5% of the total statistical error.

Figure 6(a) shows a two-dimensional scatter plot of triton energy versus proton-decay energy gated on events with $\theta \approx 0°$ for the prompt peak in the timing spectrum. The loci for decay of the IAS, GTR, and SDR to the ground state and low-lying neutron-hole states in ^{207}Pb

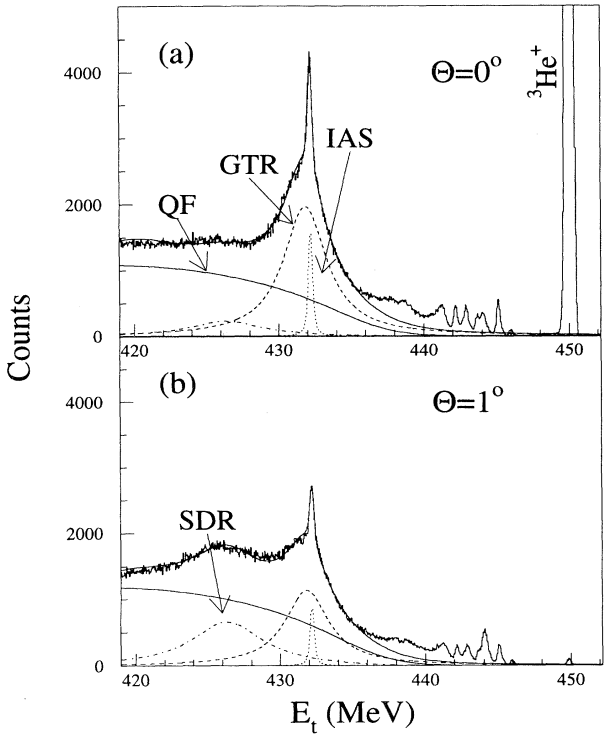

FIG. 4. Experimental triton energy spectra from the ^{208}Pb(^{3}He,t) reaction at $E(^3\text{He})$=450 MeV. (a) Spectrum gated for scattering angles centered at $\theta = 0°$. Here, the IAS, GTR, and ^{3}He$^+$ peaks are prominent. The dashed, dotted, dot-dashed, and solid lines represent the results of χ^2 fits obtained for the GTR, IAS, SDR, and nonresonant background, respectively. (b) Same as (a) but for spectrum gated for scattering angles centered at $\theta = 1°$.

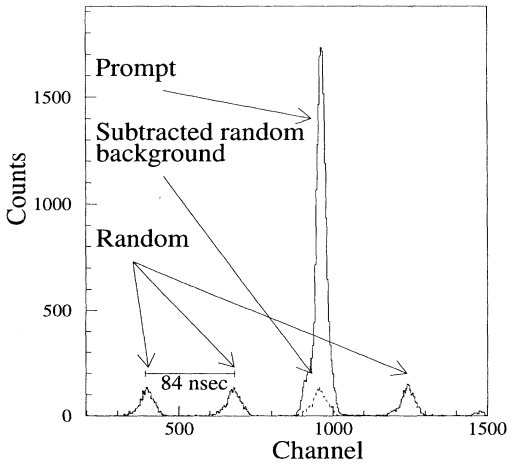

FIG. 5. Timing spectrum for the triton-proton coincidence measurements. The prominent peak corresponds to prompt coincidence events. The width of the prompt peak is 10 ns full width at half maximum. The hatched peaks correspond to random coincidence events.

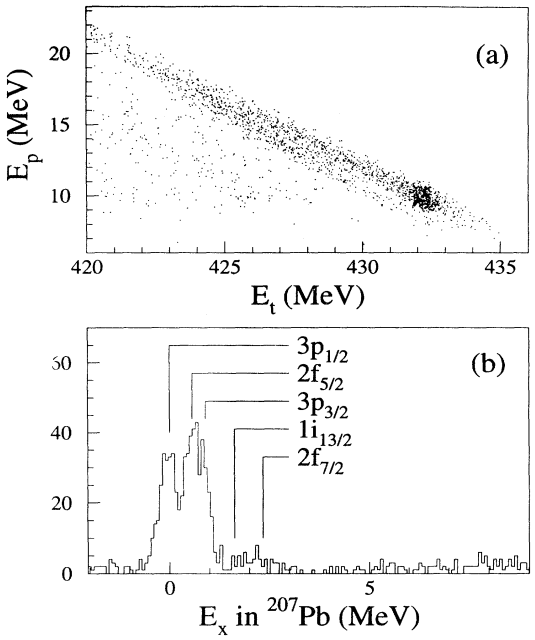

FIG. 6. (a) Two-dimensional scatter plot for prompt events of proton energy versus triton energy gated on scattering angles centered at 0°. The loci indicate decay of states in ^{208}Bi by protons to final neutron-hole states in ^{207}Pb. (b) The final-state spectrum of neutron-hole states populated in ^{207}Pb is obtained from projecting loci of part (a) onto the ^{207}Pb excitation-energy axis.

(i.e., $3p_{1/2}$, $2f_{5/2}$, $3p_{3/2}$, $1i_{13/2}$, $2f_{7/2}$) can be observed along lines corresponding to $E_t + E_p$ =const. The total energy resolution for $E_t + E_p$ was about 400 keV. This energy resolution was not sufficient to resolve completely the decays to the first and second excited states of ^{207}Pb at E_x=570 keV and 898 keV, respectively.

Figure 6(b) shows the final neutron-hole-state spectrum in ^{207}Pb obtained by projecting the events from Fig. 6(a) onto the axis of excitation energy for ^{207}Pb. This figure was obtained by further applying a gate on the excitation energy region of the GTR and IAS in ^{208}Bi. Here, various peaks correspond to proton decays to the final states in ^{207}Pb.

Triton-energy spectra gated on the final neutron-hole states in ^{207}Pb (E_x=0 to 4 MeV) are shown in Fig. 7 for scattering angles centered at 0° [Fig. 7(a)] and 1° [Fig. 7(b)]. In Fig. 6(b) and Fig. 7, contributions from random coincidences were removed by subtracting random events from the prompt events both projected by gating on the respective peaks in the timing spectrum between tritons and protons (see Fig. 5).

IV. DATA ANALYSIS

A. Singles spectra

The singles spectra of Fig. 4 were decomposed into resonances and nonresonant background by a least-squares

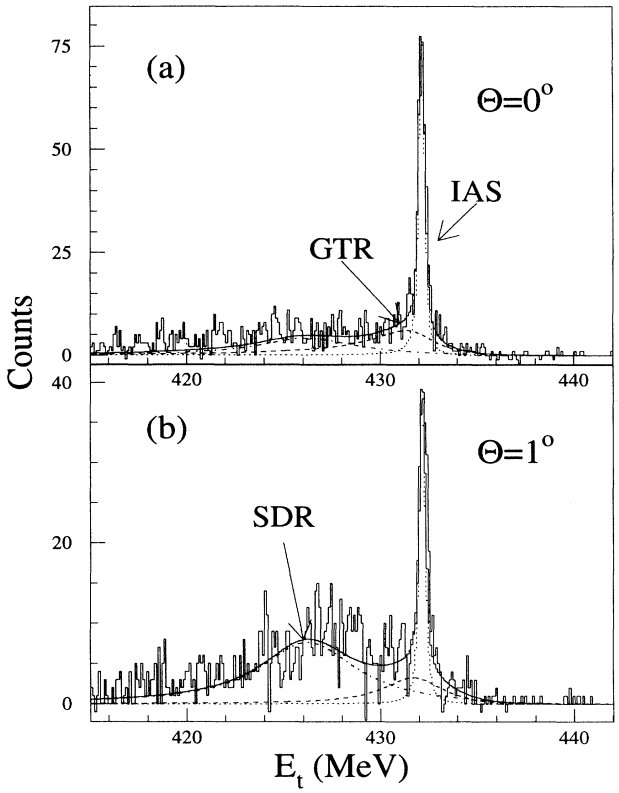

FIG. 7. Experimental triton energy spectra gated on proton decay to the neutron-hole states in ^{207}Pb. The dashed, dotted, and dot-dashed lines represent the fits obtained for the GTR, IAS, and SDR in ^{208}Pb, respectively. Spectra are gated on scattering angles centered at 0° (a) and 1° (b).

fitting procedure. The singles ^{208}Pb(^{3}He,t) spectra at 0° and 1° were assumed to consist of four components each, the Gamow-Teller resonance, the isobaric analog resonance, the spin-flip dipole resonance, and the nonresonant background.

A quasifree charge-exchange reaction is the main source of nonresonant continuum background. A semiphenomenological model was applied in the studies of pion-induced charge-exchange reactions by Erell *et al.* [31]. This model was successfully applied to describe the shape of the continuum background in the Sn(^{3}He,t) reactions [32,33]. In this model, the shape of the quasifree (QF) peak was represented by a product of a Breit-Wigner and a cutoff function. This is expressed as

$$\frac{d^2\sigma_{\rm QF}}{dEd\Omega} = N_{\rm QF}\frac{1-\exp[(E_t-E_0)/T]}{1+[(E_t-E_{\rm QF})/W]^2}. \quad (1)$$

Here, the centroid energy $E_{\rm QF}$ in the Breit-Wigner shape function is shifted relative to the value for the free process E_t(free) by the proton binding energy S_p, the excitation energy of the residual neutron-hole state $E_x^{(n)}$, and the Coulomb barrier for the proton $B_{\rm Coul}$, hence $E_{\rm QF} = E_t({\rm free}) - (S_p + E_x^{(n)} + B_{\rm Coul})$. The width W is due to the Fermi motion of neutrons inside the target nucleus. The exponential cutoff term results from Pauli blocking. The quantity T has the characteristics of a temperature. The cutoff energy $E_0 = E_t({\rm free}) - S_p$ is determined by the three-body breakup energy. The values of T and W were fixed at 100 MeV and 22 MeV, respectively, according to the previous result for tin isotopes [32]. The calculated shape and therefore the yield of the resonances was rather insensitive to T and W. The value of $E_{\rm QF}$ was also fixed at 430.4 MeV. This value was obtained by taking into account the difference in the Coulomb barrier between lead and tin nuclei.

In the fitting procedure, Breit-Wigner line shapes were assumed for the resonance shapes. The yields, the widths, and the excitation energies of the GTR, IAS, and SDR were searched for as free parameters. Since the width of the IAS (232 keV [34]) was of the same order of magnitude compared with the energy resolution of the measurement (300 keV), the Breit-Wigner function for the IAS was folded with an experimental energy distribution function. This function was assumed to be a Gaussian, the shape of which was determined by fitting the low-lying discrete levels in ^{208}Bi and the ^{3}He$^+$ peak. No folding was necessary for the GTR and the SDR. The shape functions used in the present analysis are given as

$$\frac{d^2\sigma_{\rm GTR}}{dEd\Omega} = \frac{N_{\rm GTR}}{2\pi\Gamma_{\rm GTR}}\frac{1}{1+(\frac{E_t-E_{\rm GTR}}{\Gamma_{\rm GTR}/2})^2}, \quad (2)$$

$$\frac{d^2\sigma_{\rm SDR}}{dEd\Omega} = \frac{N_{\rm SDR}}{2\pi\Gamma_{\rm SDR}}\frac{1}{1+(\frac{E_t-E_{\rm SDR}}{\Gamma_{\rm SDR}/2})^2}, \quad (3)$$

$$\frac{d^2\sigma_{\rm IAS}}{dEd\Omega} = \frac{N_{\rm IAS}}{2\pi N_0\Gamma_{\rm IAS}}\int_{-\infty}^{\infty}\frac{\exp\left[-\frac{1}{2}(E/\sigma_0)^2\right]}{1+(\frac{E_t-E_{\rm IAS}-E}{\Gamma_{\rm IAS}/2})^2}dE. \quad (4)$$

Here, E_t is the energy of the triton. $\Gamma_{\rm GTR}$, $\Gamma_{\rm SDR}$, and $\Gamma_{\rm IAS}$ are the widths of the resonances, and $E_{\rm GTR}$, $E_{\rm SDR}$, and $E_{\rm IAS}$ are their excitation energies. $N_{\rm GTR}$, $N_{\rm SDR}$, and $N_{\rm IAS}$ give the maxima for the resonances. N_0 in Eq. (4) is a normalization factor for Gaussian integration of the line shape over E. The experimental resolution is denoted by σ_0. The triton energy spectra at 0° and 1° were fitted simultaneously. The widths and the excitation energies of the resonances were fixed at the same values for both the spectra at 0° and 1°. The number of the fitted data points was 2800. The χ^2 value per degree of freedom as a result of the fitting was 1.2.

The results of the fitting procedure at 0° and 1° are plotted in Fig. 4. The excitation energy and the total width of the GTR ($\Gamma_{\rm GTR}$) in ^{208}Bi determined from the fitting are E_x=15.6±0.2 MeV and $\Gamma_{\rm GTR}$=3.72±0.25 MeV, respectively. The excitation energy and the total width of the SDR were determined to be E_x=21.1±0.8 MeV and $\Gamma_{\rm SDR}$=8.4±1.7 MeV, respectively. The excitation energies determined for the GTR, IAS, and SDR are in good agreement with the previous results [9]. The width of the IAS was consistently reproduced by taking into account the known total width of the IAS ($\Gamma_{\rm IAS}$=232 keV) from Ref. [34] and the experimental resolution of 300 keV.

Figure 8 shows the spectra measured at several angles

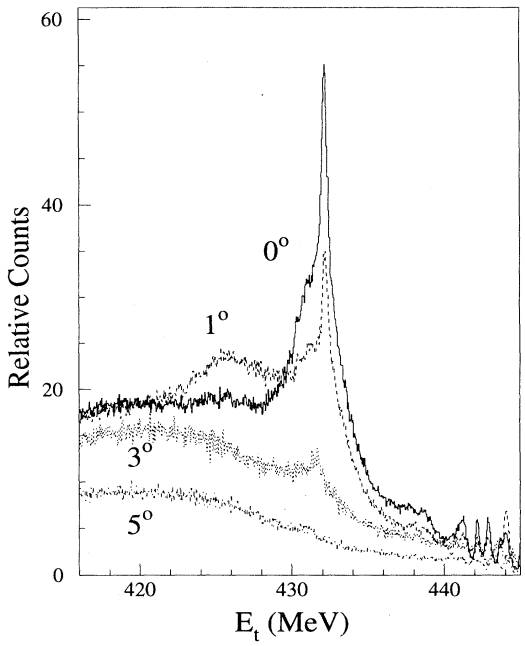

FIG. 8. Experimental triton energy spectra from the ^{208}Pb(^{3}He,t)^{208}Bi reaction at $E(^3\text{He})$=450 MeV for four scattering angles. The solid, dashed, dotted, and dot-dashed histograms correspond to the spectra measured at 0°, 1°, 3°, and 5°. All spectra are normalized by the integrated charge of the incident $^3\text{He}^{++}$ beam.

for the ^{208}Pb(^{3}He,t) reaction at 450 MeV. The singles spectra at 3° and 5° were also fitted by using the same widths and excitation energies as obtained at 0° and 1°. The differential cross sections of the GTR and the IAS have sharp peaks at 0°, which is characteristic of $\Delta L = 0$ transitions. On the other hand, the differential cross section for the SDR has the first maximum at ~1° showing the characteristic pattern of a $\Delta L = 1$ transition. The differential cross sections obtained in the (^{3}He,t) reaction at 450 MeV agree well with those of the (p,n) reaction at 200 MeV [10] if the cross sections are plotted as a function of the transferred momentum. The angular distribution of the QF peak was found to be quite flat near 0°.

The total Gamow-Teller strength, B(GT), in ^{208}Bi determined as a result of the present analysis was estimated using the cross sections of the ^{13}C(^{3}He,t)^{13}N$_{\text{g.s.}}$, and ^{13}C(^{3}He,t)^{13}N$_{3.51\ \text{MeV}}$ reactions, and the known GT and Fermi strengths of the levels in ^{13}N. The ^{13}C(^{3}He,t) reaction was measured with the same setup as for the singles ^{208}Pb(^{3}He,t) measurement. The 0° cross section for a GT transition and a Fermi transition may be factorized as [7,21],

$$\left(\frac{d\sigma}{d\Omega}\right)(\theta=0°) = \left(\frac{\mu}{\pi\hbar^2}\right)^2 \frac{k_f}{k_i}[N_{\sigma\tau}|J_{\sigma\tau}|^2 B(\text{GT}) + N_\sigma |J_\tau|^2 B(F)], \quad (5)$$

where μ is the reduced mass, k_i and k_f are the initial and final momenta, $J_{\sigma\tau}$ and J_τ are the volume integrals of the $\sigma\tau$ and τ components of the nucleon-nucleus effective interaction, B(GT) and $B(F)$ are the GT and Fermi strengths carried by the transition, and $N_{\sigma\tau}$ and N_τ are distortion factors which are ratios of the cross sections calculated in the distorted- and plane-wave Born approximations

$$N = \frac{\left(\frac{d\sigma}{d\Omega}\right)_{\text{DW}}(\theta=0°)}{\left(\frac{d\sigma}{d\Omega}\right)_{\text{PW}}(\theta=0°)}. \quad (6)$$

The ratio $|J_{\sigma\tau}/J_\tau|^2$ can be obtained using the ratio of the cross sections of known GT and Fermi transitions at 0°. The extracted ratio, $|J_{\sigma\tau}/J_\tau|^2$, from the ^{13}C(^{3}He,t)^{13}N reaction was 8.24±1.1 at $E(^3\text{He})$=450 MeV. This value is in good agreement with the ratio extracted from the ^{13}C$(p,n)^{13}$N reaction at E_p=160 MeV [35]. A ratio of the cross sections of the GTR to that of the IAS can be written following Eq. (5) as

$$R = \frac{\left(\frac{d\sigma}{d\Omega}\right)_{\text{GTR}}(\theta=0°)}{\left(\frac{d\sigma}{d\Omega}\right)_{\text{IAS}}(\theta=0°)} = \frac{k_{f(\text{GTR})}k_{i(\text{IAS})}}{k_{i(\text{GTR})}k_{f(\text{IAS})}}\frac{N_{\sigma\tau}}{N_\tau}\left|\frac{J_{\sigma\tau}}{J_\tau}\right|^2 \frac{B(\text{GT})_{\text{GTR}}}{B(F)_{\text{IAS}}}. \quad (7)$$

Here, σ_{GTR} and σ_{IAS} are the experimental 0° cross sections of the GTR and IAS in ^{208}Bi, $B(\text{GT})_{\text{GTR}}$ and $B(F)_{\text{IAS}}$ are the Gamow-Teller and Fermi strengths carried by the GTR peak and the IAS peak, respectively. In this estimate, the ratio of the distortion factors $N_{\sigma\tau}/N_\tau$ can be approximated to be unity. The IAS in ^{208}Bi exhausts 100% of the total Fermi sum rule strength $(N-Z) = 44$. Substituting the experimental ratio of the cross sections, R=15.0±3.1 and $|J_{\sigma\tau}/J_\tau|^2$=8.24±1.1 into Eq. (7), the B(GT) value carried by the GTR peak was determined to be 80±20. This value corresponds to 60±15% of the total theoretical GT sum rule strength in ^{208}Bi of $3(N-Z) = 132$. This result agrees with the quenching factor obtained for (p,n) reactions at 160 MeV [10].

B. Coincidence spectra

Coincidence spectra were also decomposed into the three resonances by a least-squares fitting procedure. Since the nonresonant yield for protons in the quasifree (^{3}He,tp) process is strongly forward peaked, the yield for coincidence events with the decay-proton detectors (SSD) located at backward angles was negligible for this process. The triton energy spectra gated on the proton decay to the neutron-hole states in ^{207}Pb is shown in Fig. 7. The continuum background from the QF process seen in the singles spectra in Fig. 4 disappears completely. Therefore, in the following analysis, only contributions from the GTR, SDR, and IAS in ^{208}Bi were considered. Triton energy spectra were obtained by gating on the decay to the neutron-hole states in ^{207}Pb, and they were fitted using the line shapes shown in Eqs. (2), (3), and (4). The results of the fits are shown in Fig. 7. Since the energy

resolution was not sufficient to separate the proton decay to the $2f_{5/2}$ and $3p_{3/2}$ levels, only their sum was further analyzed.

In the fitting procedure, a small shift of the centroid energy of the GTR towards higher excitation energy was found. The origin of this energy shift is well understood. It is due to the fact that decay of low-energy protons tends to be strongly suppressed due to the Coulomb and centrifugal barriers. In the triton spectra gated on the $3p_{1/2}$ and $(2f_{5/2} + 3p_{3/2})$ levels, the energy shifts were 130±150 keV and 720±340 keV, respectively, compared with the results of the singles spectrum. The yields of protons decaying to the $1i_{13/2}$, $2f_{7/2}$, and $1h_{9/2}$ levels were too small to establish their shifts. It can be seen from Fig. 6(a) that proton emission is strongly cut off at a proton energy of about 8 MeV.

V. RESULTS AND DISCUSSION

The total width of the giant resonances, such as the IAS and the GTR, can be written as

$$\Gamma = \Gamma^{\downarrow} + \Gamma^{\uparrow}. \tag{8}$$

Here, $\Gamma^{\downarrow}$ is the spreading width, and $\Gamma^{\uparrow}$ is the escape width which is connected with the microscopic, one-proton-particle–one-neutron-hole structure of the resonance. In heavy nuclei, such as ^{208}Bi, the spreading width leads predominantly to statistical neutron decay because statistical proton decay is strongly suppressed by the Coulomb barrier. The escape width is made up of the sum of the partial escape widths which are due to proton decays to single-neutron-hole states in the final daughter nuclei. The escape width can thus be written as

$$\Gamma^{\uparrow} = \Gamma^{\uparrow}_{p} = \sum_{i} \Gamma^{\uparrow}_{p_i}, \tag{9}$$

where $\Gamma^{\uparrow}_{p_i}$ is the partial escape width associated with decay to the ith neutron-hole state of ^{207}Pb. The ratio of $\Gamma^{\uparrow}$ to the total width Γ can be obtained from the ratio of the coincidence double-differential cross section to the singles cross section,

$$\frac{\Gamma^{\uparrow}_{p_i}}{\Gamma} = \frac{\int \frac{d^2\sigma_{p_i}}{d\Omega_t d\Omega_p} d\Omega_p}{d\sigma/d\Omega_t}. \tag{10}$$

Here, it is implicitly assumed that the double-differential singles cross sections have been integrated over the excitation energy of the resonance.

The experimental angular correlation patterns for proton decay relative to the triton emission angle at 0° are shown for the IAS and the GTR in Fig. 9. The angular correlation pattern can in general be described using Legendre polynomials. For a 1^+ state it is given by $1 + a_2P_2$. The coefficients a_2 for the proton decay from the GTR to the $3p_{1/2}$ and $(2f_{5/2} + 3p_{3/2})$ states are consistent with zero from fitting the 132° and 157° data points. The coefficients a_2 for the proton decay to the $1i_{13/2}$ and $2f_{7/2}$ states are also consistent with zero, although in these cases the uncertainties are large because of poor statistics. The angular correlation for the 0^+, IAS is also consistent with isotropy within the statistical errors. These results concerning the angular correlation patterns are expected since the decays of the GTR and IAS must be isotropic because of the $\Delta L = 0$ transfer.

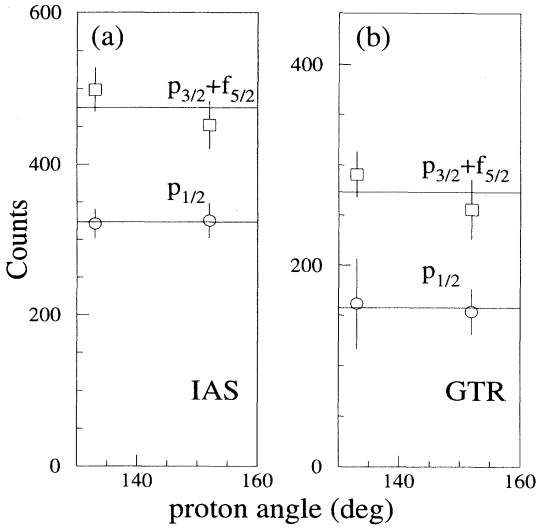

FIG. 9. Angular correlation patterns for proton decay from the IAS (a) and GTR (b) in ^{208}Bi. The 0° axis is taken as the direction of triton emission in the ^{208}Pb(^{3}He,tp)^{207}Pb reaction. The plotted points are labeled for the decay to the $3p_{1/2}$ (○) and $3p_{3/2} + 2f_{5/2}$ (□) neutron-hole states in ^{207}Pb. The solid lines are shown to guide the eye.

The measured branching ratios and the partial escape widths of the GTR and IAS are given in Table I in columns 9 and 10 and in Table II in columns 9 and 10, respectively. Here, $\Gamma_{\rm GTR}$=3.72 MeV was used for the total width of the GTR. For the total width of the IAS, $\Gamma_{\rm IAS}$=232 keV was taken from Ref. [34]. The previous experimental values for the partial escape widths are also listed in Table I in column 8 for the GTR [22] and in Table II in column 8 for the IAS [36].

The present partial escape widths for the IAS [36] agree very well with the previous data. This result implies that the extraction of the escape width in the present experiment is reliable. On the other hand, the escape widths of the GTR obtained in the present (^{3}He,t) experiment are in disagreement with the previous results at 27 MeV/u [22]. This can be attributed to the fact that the excitation of the GTR is quite weak for bombarding energies of <100 MeV/u. At low bombarding energies, other processes, including those discussed in the introduction, can contribute to the triton-proton coincidence yield making it difficult to extract a reliable escape width for the GTR.

Results of theoretical calculations for the IAS and GTR within the framework of continuum Tamm-Dancoff approximation (TDA) with Skyrme-type interactions by Colò *et al.* [37] are listed in Tables I and II in columns 3–6. In their calculations, the spreading effect was taken into

TABLE I. Theoretical and experimental partial escape widths and branching ratios for the decay of GTR in ^{208}Bi into neutron-hole states in ^{207}Pb. All widths are given in keV.

Decay channel	E_x[a] (keV)	Theor. $\Gamma^{\uparrow}_{p_i}/\Gamma$ (Ref. [37]) b	c	d	e	Expt.[f] $\Gamma^{\uparrow}_{p_i}/\Gamma^{f}$	$\Gamma^{\uparrow}_{p_i}$	Expt.[g] $\Gamma^{\uparrow}_{p_i}/\Gamma^{g}$	$\Gamma^{\uparrow}_{p_i}$
$3p_{1/2}$	0	0.037	0.022	0.033	0.018	0.132±0.016	570±70	0.018±0.005	58.4±19.8
$2f_{5/2}$	570	0.051	0.030	0.013	0.007	incl. in $p_{3/2}$	incl. in $p_{3/2}$	incl. in $p_{3/2}$	incl. in $p_{3/2}$
$3p_{3/2}$	898	0.055	0.033	0.035	0.019	0.261±0.069	1130±300	0.027±0.006	101.5±31.3
$1i_{13/2}$	1633	0.001	0.001	0.003	0.001	0.411±0.115	1780±500	0.002±0.002	8.3±9.4
$2f_{7/2}$	2340	0.009	0.005	0.010	0.003	0.196±0.069	850±300	0.004±0.002	15.6±7.6
$1h_{9/2}$	3413	0.001	0.001	0.001	$< 10^{-3}$				
$\sum_i \Gamma^{\uparrow}_{pi}/\Gamma$		0.154	0.092	0.095	0.048	~1.00	~4330	0.049±0.013	184±49
Γ		3000	3000	3100	3100		4330		3720

[a]Nuclear Data Sheet.
[b]Obtained with SIII interaction. The final state is a pure HF configuration.
[c]Obtained with SIII interaction, employing empirical proton emission energies and neutron spectroscopic factors.
[d]As Footnote b but with SGII interaction.
[e]As Footnote c but with SGII interaction.
[f]Reference [22].
[g]Present experimental results.

account by introducing a coupling to collective vibration modes. Columns 3 and 5 display the partial proton escape widths obtained in pure Hartree-Fock calculations. Columns 4 and 6 are the results obtained after setting proton emission energies and neutron spectroscopic factors to the experimental values. The theoretical calculations for the proton decay from the IAS reproduce the experimental values reasonably only if the SIII interaction is used.

The total width, escape widths, and excitation energy of the IAS are not much affected by introducing the spreading effect, because spreading is mediated by coupling to the isovector monopole resonance via the Coulomb interaction and because neutron decay of the IAS is suppressed by isospin selection rules. The experimental branching ratio for statistical neutron decay is only 37±3% [38]. This is consistent with the experimental result for the proton-decay branching ratio of 63±3% [22]. However, the spreading effect is more important for the GTR because spreading is mediated by coupling to the underlying $2p$-$2h$ states via the strong interaction leading to an experimental branching ratio for direct proton decay of only 4.9±1.3%.

Colò *et al.* [37] and Udagawa *et al.* [39] pointed out that when the spreading effect is included semiempirically in the theoretical calculations, the total strength of the GTR residing in the main component is reduced to 60% of the sum rule value $3(N-Z)$. Furthermore, the total width of the GTR and the distribution of the GT strength are significantly modified. Theoretical calcula-

TABLE II. Theoretical and experimental partial escape widths and branching ratios for the decay of IAS in ^{208}Bi into neutron-hole states in ^{207}Pb. All widths are given in keV.

Decay channel	E_x[a] (keV)	Theor. $\Gamma^{\uparrow}_{p_i}/\Gamma$ (Ref. [37]) b	c	d	e	Expt.[f] $\Gamma^{\uparrow}_{p_i}/\Gamma^{f}$	$\Gamma^{\uparrow}_{p_i}$	Expt.[g] $\Gamma^{\uparrow}_{p_i}/\Gamma^{g}$	$\Gamma^{\uparrow}_{p_i}$
$3p_{1/2}$	0	0.346	0.237	0.171	0.137	0.224±0.007	51.9±1.6	0.22±0.03	52.3±9.5
$2f_{5/2}$	570	0.086	0.061	0.008	0.006	0.114±0.009	26.4±2.0	incl. in $p_{3/2}$	incl. in $p_{3/2}$
$3p_{3/2}$	898	0.287	0.196	0.198	0.157	0.279±0.015	64.7±3.4	0.34±0.06	80.9±15.3
$1i_{13/2}$	1633	0.011	0.010	0.007	0.006			-	-
$2f_{7/2}$	2340	$< 10^{-3}$	$< 10^{-3}$	0.002	0.004	0.018±0.003	4.2±0.6	0.015±0.007	3.6±1.7
$1h_{9/2}$	3413	$< 10^{-3}$	$< 10^{-3}$	$< 10^{-3}$	$< 10^{-3}$			-	-
$\sum_i \Gamma^{\uparrow}_{pi}/\Gamma$		0.730	0.504	0.386	0.310	0.63±0.03	147.2±7.0	0.58±0.09	136.8±21.8
Γ		152	152	99	99		232[h]		232[h]

[a]Nuclear Data Sheet.
[b]Obtained with SIII interaction. The final state is a pure HF configuration.
[c]Obtained with SIII interaction, employing empirical proton emission energies and neutron spectroscopic factors.
[d]As Footnote b but with SGII interaction.
[e]As Footnote c but with SGII interaction.
[f]Reference [36].
[g]Present experimental results.
[h]Taken from Ref. [34].

tions with pure Hartree-Fock wave functions [37] give an excitation energy for the GTR that is higher than the experimental value by about 2 to 3 MeV. The proton decay branching ratios, which are deduced by employing empirical proton emission energies and neutron spectroscopic factors, depend on the choice of the interaction parameters in the calculations. The calculation with the SGII interaction well reproduce the experimental values. However, for the IAS, the calculations with the SGII interaction underestimate the experimental ratios.

As mentioned above, the shift of the centroid energy of the GTR observed in the coincidence spectra is caused by the suppression of low-energy proton emission due to the Coulomb and centrifugal barriers. This means that the partial escape widths are sensitive to the excitation energy of the GTR.

Recent calculations by Muraviev and Urin [40] in RPA, with coupling to the continuum and with the strength of the Landau-Migdal force given by $g'=1.2$, reproduce the experimental results reasonably well when the experimental proton escape energies are used. A better agreement is obtained if $g'=1.4$ is taken. However, this choice of g' does not agree with the normal value of the Landau-Migdal parameter [41].

Udagawa *et al.* [39] calculated the partial escape widths of the GTR within the framework of the continuum TDA. In their calculation, the spreading effect was taken into account by introducing the imaginary part of the optical potential. They pointed out that the GT strength function was similar to the strength function obtained by taking into account the coupling to the $2p$-$2h$ states [42]. An explicit treatment of the direct particle decay and the coupling to the $2p$-$2h$ states seems to be necessary in order to understand the damping as well as the quenching mechanisms of the GTR [43].

The partial proton escape widths for the decay of the SDR in ^{208}Bi to the various neutron-hole states in ^{207}Pb have not been determined since the energy resolution for the emitted high-energy protons was not sufficient to resolve the decay to these final states. However, one can infer from the final-state spectra (not shown here) that the population pattern of the various neutron-hole states is different for the SDR than that for the GTR, in that the $1i_{13/2}$ and $2f_{7/2}$ are more strongly and the $3p_{1/2}$ more weakly populated. Furthermore, the total proton decay branching ratio for the SDR has been determined from the coincidence spectra to be $14.1 \pm 4.2\%$. If assumed to result from the decay of one single resonance with a width of 8.4 ± 1.7 MeV, this would lead to a total proton escape width of 1.18 ± 0.35 MeV.

The observed SDR is expected to consist of three spin components, i.e., 2^-, 1^-, and 0^-. These components are expected to have excitation energies $E_x(2^-) < E_x(1^-) < E_x(0^-)$ with the strength ratio of 5:3:1. It was not possible in the present experiment to disentangle the various spin components (2^-, 1^-, and 0^-) of the SDR on the basis of their angular correlation patterns. Even if one assumes that the observed total proton escape width should be divided among these three components, the resulting proton escape width per component is still considerably larger than that for the GTR. This can be understood qualitatively by taking into account the increase of the proton energy available above the Coulomb barrier and also the average decrease of the centrifugal barrier for the decay protons as compared to the GTR. There are also indications for proton decay to the broad $1h_{9/2}$ deep-neutron-hole state in ^{207}Pb. A better understanding of these observations awaits further theoretical efforts.

VI. SUMMARY

We have reported the first successful measurement of proton decay from a Gamow-Teller resonance (GTR) performed with the ^{208}Pb(^{3}He,tp) reaction at $E(^3\text{He})=450$ MeV. The partial and total branching ratios for direct proton decay of the Gamow-Teller resonance and isobaric analog state were determined. The total branching ratio for direct proton decay of the spin-flip dipole resonance was also determined. The deduced partial escape widths of the IAS are in good agreement with the earlier data. Theoretical calculations based on the continuum TDA reproduce the experimental values very well. This means that a good understanding of the microscopic structure of the IAS has been established. However, the previous data obtained at $E(^3\text{He})=81$ MeV [22] for the partial escape widths of the GTR are in complete disagreement with theoretical calculations based on the continuum TDA. On the other hand, these calculations reproduce the experimental data obtained in the present work reasonably well suggesting a basic understanding of the damping mechanism of the GTR. Our experimental results for the SDR suggest that further theoretical work is needed to understand the microscopic structure of spin-flip $\Delta L = 1$ collective excitations in nuclei, and to explain why the branching ratios for proton decay from ^{208}Bi are higher for these excitations than they are for the spin-flip GTR.

ACKNOWLEDGEMENTS

The authors are grateful to the RCNP cyclotron staff for their support in the present experiment. The present work was performed in part under the U.S.-Japan Cooperative Science Program supported by the U.S. National Science Foundation (NSF) and by the Japan Society for the Promotion of Science (JSPS). Two of the authors (M.N.H. and J.J.) gratefully acknowledge fellowships awarded by JSPS which made the extended visit to RCNP possible.

[1] J.I. Fujita and K. Ikeda, Nucl. Phys. **67**, 145 (1965).
[2] K. Ikeda, S. Fujii, and J.I. Fujita, Phys. Lett. **3**, 271 (1963).
[3] R.R. Doering, A. Galonsky, D.M. Patterson, and G.F. Bertsch, Phys. Rev. Lett. **35**, 1961 (1975).
[4] P.H. Bowen, C. Cox, G. Huxtable, J.P. Scanlon, J.J. Thresher, and A. Langsford, Nucl. Phys. **30**, 475 (1962).
[5] K. Ikeda, S. Fujii, and F.I. Fujita, Phys. Lett. **2**, 169 (1962).
[6] D.E. Bainum, J. Rapaport, C.D. Goodman, D.J. Horen, C.C. Foster, M.B. Greenfield, and C.A. Goulding, Phys. Rev. Lett. **44**, 1751 (1980).
[7] C.D. Goodman, C.A. Goulding, M.B. Greenfield, J. Rapaport, D.E. Bainum, C.C. Foster, W.G. Love, and F.P. Petrovich, Phys. Rev. Lett. **44**, 1755 (1980).
[8] B.D. Anderson, J.N. Knudson, P.C. Tandy, J.W. Watson, R. Madey, and C.C. Foster, Phys. Rev. Lett. **45**, 699 (1980).
[9] D.J. Horen, C.D. Goodman, C.C. Foster, C.A. Goulding, M.B. Greenfield, J. Rapaport, D.E. Bainum, E. Sugarbaker, F. Petrovich, and W.G. Love, Phys. Lett. **95B**, 27 (1980).
[10] C. Gaarde, J. Rapaport, T.N. Taddeucci, C.D. Goodman, C.C. Foster, D.E. Bainum, C.A. Goulding, M.B. Greenfield, D.J. Horen, and E. Sugarbaker, Nucl. Phys. **A369**, 258 (1981).
[11] D.J. Horen, C.D. Goodman, D.E. Bainum, C.C. Foster, C. Gaarde, C.A. Goulding, M.B. Greenfield, J. Rapaport, T.N. Taddeucci, E. Sugarbaker, T. Masterson, S.M. Austin, A. Galonsky, and W. Sterrenburg, Phys. Lett. **99B**, 383 (1981).
[12] C. Gaarde, J.S. Larsen, M.N. Harakeh, S.Y. van der Werf, M. Igarashi, and A. Müller-Arnke, Nucl. Phys. **A334**, 248 (1980).
[13] H. Ejiri, K. Ikeda, and J.I. Fujita, Phys. Rev. **176**, 1277 (1968).
[14] W.G. Love and M.A. Franey, Phys. Rev. C **24**, 1073 (1981).
[15] F. Petrovich and W.G. Love, Nucl. Phys. **A354**, 499c (1981).
[16] N.S.P. King, P.W. Lisowski, G.L. Morgan, P.N. Craig, R.G. Jeppesen, D.A. Lind, J.R. Shepard, J.L. Ullman, C.D. Zafiratos, C.D. Goodman, and C.A. Goulding, Phys. Lett. B **175**, 279 (1986).
[17] W.P. Alford, R.L. Helmer, R. Abegg, A. Celler, O. Häuser, K. Hicks, K.P. Jackson, C.A. Miller, S. Yen, R.E. Azuma, D. Frekers, R.S. Henderson, H. Baer, and C.D. Zafiratos, Phys Lett. B **179**, 20 (1986).
[18] T.N. Taddeucci, C.A. Goulding, T.A. Carey, R.C. Byrd, C.D. Goodman, C. Gaarde, J. Larsen, D. Horen, J. Rapaport, and E. Sugarbaker, Nucl. Phys. **A469**, 125 (1987).
[19] S. Yoshida and S. Adachi, Z. Phys. A **325**, 411 (1986).
[20] C. Ellegaard, C. Gaarde, J.S. Larsen, C. Goodman, I. Bergqvist, L. Carlèn, L.P. Ekström, B. Jakobsson, J. Lyttkens, M. Bedjidian, M. Chamcham, J.Y. Grossiord, A. Guichard, M. Gusakow, R. Haroutunian, J.R. Pizzi, D. Bachelier, J.L. Boyard, T. Hennino, J.C. Jourdain, M. Roy-Stephan, M. Boivin, and P. Radvanyi, Phys. Rev. Lett. **50**, 1745 (1983).
[21] I. Bergqvist, A. Brockstedt, L. Carlèn, L.P. Ekström, B. Jakobsson, C. Ellegaard, C. Gaarde, J.S. Larsen, C. Goodman, M. Bedjidian, D. Contardo, J.Y. Grossiord, A. Guichard, R. Haroutunian, J.R. Pizzi, D. Bachelier, J.L. Boyard, T. Hennino, J.C. Jourdain, M. Roy-Stephan, M. Boivin, and P. Radvanyi, Nucl Phys. **A469**, 648 (1987).
[22] C. Gaarde, J.S. Larsen, A.G. Drentje, M.N. Harakeh, and S.Y. van der Werf, Phys. Rev. Lett. **46**, 902 (1981).
[23] M. Fujiwara, H. Akimune, I. Daito, H. Ejiri, Y. Fujita, M.B. Greenfield, M.N. Harakeh, R. Hazama, T. Inomata, J. Jänecke, N. Kudomi, S. Nakayama, K. Shinmyo, A. Tamii, M. Tanaka, H. Toyokawa, and M. Yosoi, Nucl. Phys. **A577**, 43c (1994).
[24] H. Akimune, I. Daito, Y. Fujita, M. Fujiwara, M.B. Greenfield, M.N. Harakeh, T. Inomata, J. Jänecke, K. Katori, S. Nakayama, H. Sakai, M. Tanaka, and M. Yosoi, Nucl. Phys. **A569**, 255c (1994).
[25] N. Van Giai, P.F. Bortignon, A. Bracco, and R.A. Broglia, Phys. Lett. B **233**, 1 (1989).
[26] H. Akimune, I. Daito, Y. Fujita, M. Fujiwara, M.B. Greenfield, M.N. Harakeh, T. Inomata, J. Jänecke, K. Katori, S. Nakayama, H. Sakai, M. Tanaka, and M. Yosoi, Phys. Lett. B **323**, 107 (1994).
[27] I. Miura, T. Yamazaki, A. Shimizu, K. Hosono, T. Itahashi, T. Saito, A. Ando, K. Tamura, K. Hatanaka, M. Kibayashi, M. Uraki, H. Ogata, M. Kondo, and H. Ikegami, RCNP Annual Report (1991), p. 149.
[28] M. Fujiwara, in Proceedings of the 5th French-Japanese Symposium on Nuclear Physics, Dogashima, Japan, 1989 (unpublished), p. 348.
[29] T. Noro, M. Fujiwara, O. Kamigaito, S. Hirata, Y. Fujita, A. Yamagoshi, T. Takahashi, H. Akimune, Y. Sakemi, M. Yosoi, H. Sakaguchi, and J. Tanaka, RCNP Annual Report (1991), p. 177.
[30] K. Dennis, H. Akimune, G.P.A. Berg, S. Chang, B. Davis, M. Fujiwara, M.N. Harakeh, J. Jänecke, J. Liu, K. Pham, D.A. Roberts, and E.J. Stephenson, Phys. Rev. A **50**, 3992 (1994).
[31] A. Erell, J. Alster, J. Lichtenstadt, M.A. Moinester, J.D. Bowman, M.D. Cooper, F. Irom, H.S. Matig, E. Piasetzky, and U. Sennhauser, Phys. Rev. C **34**, 1822 (1986).
[32] J. Jänecke, K. Pham, D.A. Roberts, D. Stewart, M.N. Harakeh, G.P.A. Berg, C.C. Foster, J.E. Lisantti, R. Sawafta, E.J. Stephenson, A.M. van den Berg, S.Y. van der Werf, S.E. Muraviev, and M.H. Urin, Phys. Rev. C **48**, 2828 (1993).
[33] K. Pham, J. Jänecke, D.A. Roberts, M.N. Harakeh, G.P.A. Berg, S. Chang, J. Liu, E.J. Stephenson, B.F. Davis, H. Akimune, and M. Fujiwara, Phys. Rev. C **51**, 526 (1995).
[34] R. Melzer, P. von Brentano, and H. Paetz gen. Schieck, Nucl. Phys. **A432**, 363 (1985).
[35] T.N. Taddeucci, in *The Interaction Between Medium Energy Nucleons*, edited by H.O. Meyer, AIP Conf. Proc. No. 97 (AIP, New York, 1982), p. 228.
[36] S.Y. van der Werf, M.N. Harakeh, and E.N.M. Quint, Phys. Lett. B **216**, 15 (1989), and references therein.
[37] G. Colò, N. Van Giai, P.F. Bortignon, and R.A. Broglia, Phys. Rev. C **50**, 1496 (1994).
[38] J.A. Bordewijk, A. Balanda, D. Beaumel, J. Blomgren, S. Brandenburg, G. van 't Hof, M.N. Harakeh, M.A. Hofstee, J. Jänecke, A. Krasznahorkay, H. Laurent, L. Nilsson, N. Olsson, R. Perrino, R. Siebelink, P.O. Söderman, S.Y. van der Werf, and A. van der Woude, Nucl. Phys. **A453**, 453 (1994).
[39] T. Udagawa, D.P. Knobles, and S.A. Stotts, Nucl. Phys.

A577, 67c (1994).
[40] S.E. Muraviev and M.G. Urin, Nucl. Phys. **A572**, 267 (1994); and Proceedings of IV International Conference on Selected Topics in Nuclear Structure, Dubna, Russia, 1994 (unpublished).
[41] A. Arima, K. Shimizu, W. Bentz, and H. Hyuga, Adv. Nucl. Phys. **18**, 1 (1987).
[42] S. Drozdz, S. Nishizaki, J. Speth, and J. Wambach, Phys. Rep. **197**, 1 (1990).
[43] F. Osterfeld, Rev. Mod. Phys. **64**, 64 (1992).

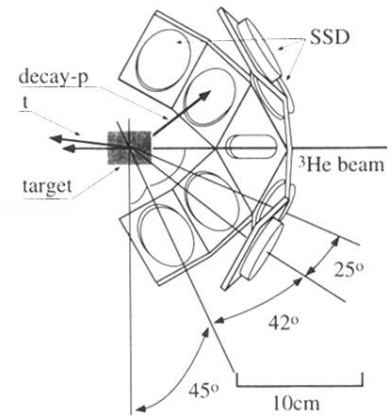

FIG. 2. Schematic picture of the layout of the SSD's.